Microgrid for radio access network resilience against power grid outages: Design and operation

Computer Networks 279 (2026) 112116

Contents lists available at ScienceDirect

Computer Networks

journal homepage: www.elsevier.com/locate/comnet

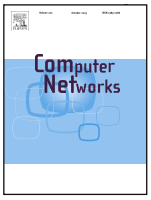

Microgrid for radio access network resilience against power grid outages: Design and operation

Greta Vallero *, Michela Meo, Umberto Brozzo Doda

Politecnico di Torino, Italy

ARTICLE INFO

Keywords:
Resilience
Microgrid
Base station
Renewable energy sources
Power grid outage
Radio access network

ABSTRACT

The continuous increase in electricity demand, combined with factors such as political instability, cyberattacks, and the rising frequency of natural disasters linked to climate change, poses significant challenges to the reliability and stability of the power grid. Failures in the power grid can have cascading effects on the communication infrastructure, which heavily depends on a stable electricity supply. Enhancing the resilience of computing and communication facilities is therefore essential to support critical aspects of daily life. To address this, we view a group of Base Stations (BSs) in a Radio Access Network (RAN) as consumers and producers within a Micro Grid (MG) equipped with Photovoltaic (PV) panels, energy storage, and interconnected by dedicated power cables for energy exchange. We propose novel RAN resource and energy management strategies designed to maximize RAN Quality of Service (QoS) during Power Grid Outages (PGOs), given the available energy within the MG. Our evaluation considers factors such as the number of BSs in the MG, PV panel capacity, PGO duration, BS traffic profiles, PV panel placement, the energy battery employment, and the geographical extent of the MG. Results demonstrate that the proposed methodology improves QoS, increasing the hourly *Managed Traffic* by up to more than 300%, an improvement obtained when the MG consists of 4 2-kWp-PV-equipped BSs, compared with isolated 2 kWp PV-equipped BSs, during daily hours. When the MG is implemented, small PV panels ($\leq$ 6kWp) perform comparably to large ones ($\geq$ 12kWp) in isolated BS setups, making the solution space-efficient. Additionally, performance is mostly unaffected by BS traffic profiles or PGO duration. Effective energy management, accounting for cable losses, and the central placement of PV panels within the MG are critical for optimizing performance.

1. Introduction

Between 2010 and 2022, reported service outages in Europe's communication networks increased by 155% [1]. In 2021, the measure of service impact, expressed as lost user hours (the product of outage duration and affected users), reached 5106 million hours, over 2.6 times higher than what was recorded in 2010 [1]. According to [1], BSs within the RAN are among the network components most impacted by these disruptions. Approximately 30% of these outages are attributed to power grid failures, highlighting the communication infrastructure's dependence on a stable electricity supply. Maintaining this continuity of power is becoming increasingly difficult due to rising electricity demand, political instability, cyberattacks, and climate change, which intensifies natural disasters and strains grid operations. Despite these challenges, computing and communication systems have become essential for everyday utilities, making their reliable, uninterrupted operation crucial even beyond standard operational conditions.

Thus, computing and communication infrastructures must be not only *reliable*, providing consistent and dependable performance, and *robust*, withstanding potential system stresses, but also *resilient* in the face of disruption. The literature offers no common definition of RAN resilience. In [2], it is defined as the ability to adapt to external changes that may alter system behavior and to swiftly recover after operational interruptions. In [3], it is described as the availability of hardware and radio resources for service over time. Other works focus on *survivability*, a subfield of resilience that addresses attacks and large-scale disasters in wired networks [4], often quantified through the loss probability or the delay distribution of non-lost packets [5]. The discussion in [6] defines network resiliency as the ability to absorb adverse impacts, adapt to them, and quickly recover to maintain an acceptable level of service from the users' perspective.

To enhance RAN resilience, the works presented in [7–12] envision the use of Open RAN, network virtualization, and roaming as promising solutions to ensure continuity of RAN service despite disruptive events.

* Corresponding author.
E-mail address: greta.vallero@polito.it (G. Vallero).

https://doi.org/10.1016/j.comnet.2026.112116
Received 21 February 2025; Received in revised form 5 February 2026; Accepted 11 February 2026
Available online 15 February 2026

Nevertheless, in the case of energy grid shortages, these solutions become ineffective because devices cannot operate without power. During PGOs, network devices rely on costly battery backup systems that act as alternative power sources during temporary grid failures [13]. However, the effective design of such systems requires careful consideration of battery placement and lifespan to minimize service disruptions [13]. Moreover, in RANs, the situation is particularly critical due to the widespread distribution and high number of BSs. With the recent increase in BS density, relying solely on backup batteries leads to high capital and maintenance costs. To address this issue, an emerging trend considers the integration of Renewable Energy Sources (RESs) located near the BSs to enhance network resilience. When designed effectively, RESs reduce the network's dependence on the power grid, mitigating the potential cascading effects of PGOs. In recent years, there has been substantial growth in the deployment of RESs, as demonstrated by the installation of 167 GW of distributed PV systems worldwide between 2019 and 2021 [14]. This expansion was largely driven by the first global energy crisis, which caused sharp increases in gas and coal prices, responsible for about 90% of the rise in global electricity costs [15]. Meanwhile, the ongoing deployment of RESs is motivated by the need to combat climate crises and achieve the ambitious goal of net-zero emissions by 2050 [16]. In this context, the concept of MGs has gained increasing attention within conventional power grids. MGs are characterized as low-voltage, small-scale electricity networks that integrate diverse distributed RESs, which can operate in a coordinated manner to effectively balance local energy supply and demand [17,18].

In the literature, powering BSs through RESs has emerged as an attractive solution to make the RAN more sustainable and self-sufficient, while also reducing operational energy costs [19–22]. While the benefits in terms of sustainability, self-sufficiency, and cost reduction have been well demonstrated, the potential of powering BSs with RESs to mitigate the effects of PGOs on mobile communication services has not yet been explored [13]. Our prior works [23,24] demonstrate that using a PV panel as an energy backup system can effectively alleviate the impact of PGOs on mobile communication services. This paper builds upon our prior work in [24], where we enhanced RAN resilience during PGOs by organizing BSs into MGs, improving the resilience of the RAN compared to traditional battery-based backup solutions. These MGs use dedicated power cables to share energy generated by PV panels installed near the BSs. This configuration enables an adaptive RAN resource and energy management strategy that prioritizes the most heavily loaded BSs during a PGO, maintaining active communication services until the MG generates enough energy to sustain operations, thereby improving RAN resilience.

In this paper, we extend our initial design by proposing additional energy management strategies that integrate batteries into the power supply system alongside the PV panels, with the objective of further improving RAN resilience against PGOs, whose cascading effects can interrupt RAN service due to energy shortages. We also analyze how the positioning of these energy components affects overall system resilience. Our analysis, based on real traffic demand data from which actual BS power demand profiles are derived, real PV panel energy production data, and real PGO records, shows that the proposed methodology is highly effective. Simulation results indicate a significant increase in the fraction of time that BSs remain operational during prolonged PGOs, compared to a benchmark scenario using conventional battery-based backup systems. Moreover, results reveal that grouping BSs into MGs, when energy is properly managed, leads to an increase of more than 300% in hourly served traffic compared to the benchmark approach that considers isolated BSs, where each BS operates independently without MG coordination, as observed in daily scenarios where each BS is equipped with a 2 kWp PV panel. Through simulations, we evaluate the impact on QoS of several factors, including the number of BSs in each MG, PV panel capacity, PGO start time, traffic demand profiles, PV panel placement, battery integration, and the distance among BSs. To the best of our knowledge, this is the first study to provide a detailed investigation of microgrid-based energy sharing as a strategy to sustain mobile communication services during PGOs, extending beyond conventional renewable energy and battery backup solutions.

Table 1
Summary of state of the art approaches to RAN resilience and their limitations.

Reference	Main contribution	Limitation / gap
[2]	Defines *reliability*, *robustness*, and *resilience*.	Does not address RAN resilience under power-grid outages.
[6]	Analyzes 5G–RAN resilience via a coverage indicator.	Does not address RAN resilience under power-grid outages.
[4,25]	Hardware–centric solutions primarily for wired network resilience.	Does not address RAN resilience under power–grid outages.
[26]	Reviews resilience strategies in renewable power systems; highlights power autonomy for disaster resilience.	Does not address RAN resilience under power–grid outages.
[27]	CTMC–based model for BS fault prediction.	Does not address RAN resilience under power–grid outages.
[9–12]	National roaming to cope with emergencies.	Does not address RAN resilience under power–grid outages.
[7]	Anomaly detection and root–cause analysis using Open RAN real–time monitoring.	Not applicable under energy unavailability; does not address power–grid outages for RAN.
[8]	Network virtualization to enhance RAN resilience.	Not applicable under energy unavailability; does not address power–grid outages for RAN.
[28]	Review of approaches to improve RAN resilience, including battery installation and RES supply.	Does not consider microgrids (MG) to enhance RES–backed autonomy.
[29]	Utilization of diesel generators for RAN resilience against power–grid loss.	Does not consider MG integration to improve RES support and autonomy.
[30]	Integration of electric vehicles to support RAN power supply.	Does not consider MG integration to improve RES support and autonomy.
[23]	Integration of RES supply to support RAN resilience during grid outages.	Does not consider MG integration to improve RES support and autonomy.
[19–21,31–34]	Design and management of RAN powered by RES for sustainability, OPEX reduction, and reduced grid dependence.	Does not address RAN resilience under power–grid outages.
[24]	MG for RAN resilience.	Simplified energy management; omits losses and battery modeling.

The paper is organized as follows. Section 2 reviews related works, while Section 3 describes the scenario. In Sections 4 and 5, we detail our proposed energy management strategies and the Key Performance Indicators (KPIs) we use for their evaluation. In Section 6, we present and discuss the results of our simulations, and our findings are drawn in Section 7. Section 8 concludes our work.

2. State of the art

According to the work presented in [2], effective system design requires careful attention to both robustness and resilience. Robustness pertains to a system's capacity to maintain or restore its performance in the face of challenges and disruptions, while resilience extends this concept by including the ability to recover from unexpected events that exceed design assumptions. With the growing reliance on communication services and the imperative for uninterrupted connectivity, robustness,

and resilience have become critical in communication networks. In [2], the authors evaluate system robustness and resilience through mechanisms such as anticipation, absorption, adaptation, and rapid recovery from adverse events, while Kaada et al. in [6] analyze and quantify 5G-RAN resilience via a coverage indicator. The studies in [4,25] enhance network reliability, availability, and robustness through measures like hardware redundancy, network scalability, traffic re-routing, load balancing, interference management, and security protocols, all of which minimize single points of failure, support traffic demand growth, prevent congestion, and detect malicious attacks.

The work presented in [26] underscores the importance of power autonomy for disaster resilience, ensuring a robust power supply for telecommunications networks. Similarly, in [27], Continuous Time Markov Chains are used to model the status of a specific BS as optimal, suboptimal, or in outage, providing a framework for reliability measurement and fault prediction. Through transient and steady-state probability distributions, this work enhances reliability via root cause analysis to avoid service disruptions. Additionally, some studies advocate for national roaming to enable Mobile Network Operators to share infrastructure when needed, particularly in emergencies, as seen in cases like Ukraine's network damages or U.S. disaster responses [9–12].

The authors in [7] highlight how Open RAN facilitates network resilience, leveraging real-time network data from BSs processed by the RAN Intelligent Controller, which enables proactive anomaly detection and root cause analysis to manage issues before they escalate. Bhattacharyya et al. in [8] illustrate that network virtualization enhances RAN resilience through the ability to migrate network functions.

Traditionally, backup systems to address temporary power interruptions, which can impact communication networks, have relied on energy batteries installed across network infrastructure. These batteries typically provide 2 to 4 h of backup power and recharge only when grid power is available [28], yet they incur high costs, require substantial space, and need regular maintenance, while also being sensitive to the frequency and duration of grid outages [23]. In response, some systems have replaced BS backup batteries with diesel generators [29], and others have explored using electric vehicles as mobile energy sources to restore power during emergencies [30].

Our previous work in [23] to enhance network resilience involves integrating RESs. Incorporating RES into RAN infrastructure supports sustainability, reduces Operational Expenditures (OPEX), and decreases dependency on the power grid [19–21,31–34].

As summarized in Table 1, these works enhance system resilience, reduce OPEX, and advance RAN sustainability, but they do not fully address resilience specifically tailored for RAN against third-party failures (e.g., power grid), which could trigger cascading network effects and render software solutions, such as Open RAN and virtualization ineffective. Our prior work in [23] leverages RES installations to enhance sustainability and reduce dependency on the power grid. Through this solution, we eliminate the need for dedicated hardware infrastructure, such as backup energy storage systems (e.g., batteries), thereby avoiding installation and maintenance costs while mitigating cascade effects from power outages. Instead, we rely on existing infrastructure designed for sustainability goals. In [24], we proposed a solution that groups RAN BSs in a coordinated manner to form a MG, as outlined in [35]. This model manages RAN resources during power grid outages based on energy availability from nearby PV panels installed close to BS locations. In this paper, we expand upon our initial design by proposing additional energy management strategies that incorporate an energy battery into the power supply system alongside the PV panels. We also examine how the placement of these energy components affects overall system resilience.

3. Scenario

In this study, we focus on a subset of a RAN, comprising N BSs, forming a MG, as illustrated in Fig. 1. These BSs act as the loads and the

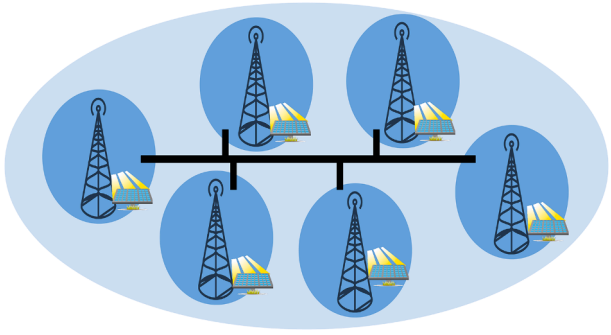

Fig. 1. The portion of RAN under consideration: it is composed of N BSs, forming a MG, that act as the loads and distribute RES energy within the MG, transferring the produced energy through dedicated cables.

Table 2
BS link budget parameters [36,37].

Parameter	2100 MHz
Frequency (MHz)	2100
Bandwidth (MHz)	120
Used Subcarriers	7680
Total Subcarriers	12,288
Sampling Factor	1536
TDD Duty Cycle DL (%)	75
TDD Duty Cycle UL (%)	25
Spatial Duty Cycle (%)	0
BS Transmit Antenna Gain (dBi)	18
BS Transmit Array Antenna Feed Loss (dBi)	2
BS Ratiated Power (dBm)	49
BS Number of Antenna Elements	1
User Antenna Element Gain (dBi)	0
User Transmit Power (dBm)	23
User Antenna Height (m)	1.5
User Number of Antenna Elements	1
Receiver Noise Figure (dB)	8

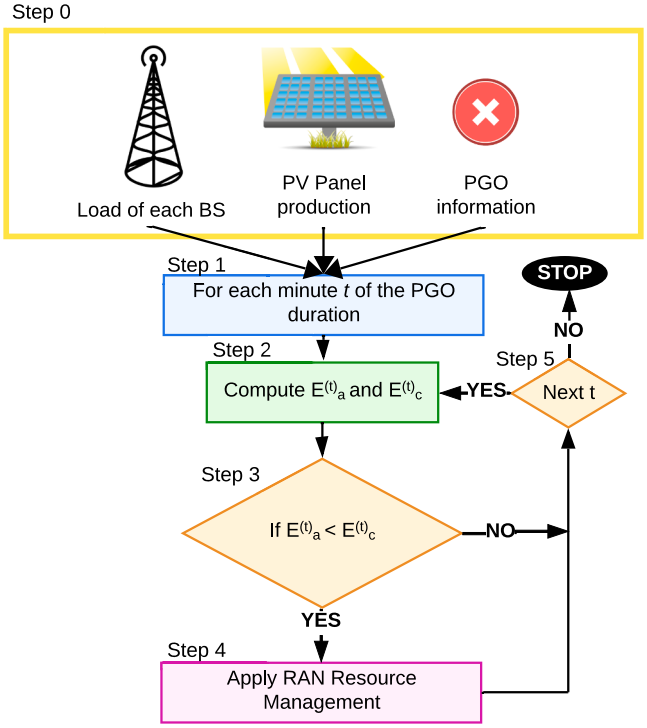

Fig. 2. Flow chart with the different steps of our simulations.

distributed RESs within the MG, transferring energy through dedicated cables, see black lines in Fig. 1. Each BS operates on 5G technology, with a frequency of 2.1 GHz and a maximum channel bandwidth of 120 MHz. Table 2 summarizes the link budget details, taken from [37]. Each BS is equipped with a PV panel system, which provides the energy for its supply. We assume a crystalline silicon technology for the PV modules and consider a DC-to-AC inverter efficiency of 96%. Given optimal tilting and azimuth angles for the location (20° and 180°, respectively), an average daily solar radiation of 4 kWh/m^2 is observed throughout the year, accounting for typical performance losses of approximately 14% in real systems. In addition, the MG has a set of energy battery units, each with a capacity of 200 Ah and a voltage of 12 V. The maximum Depth of Discharge (DOD) is 70%, which allows the battery to operate for more than 500–600 cycles before being replaced [38,39]. We consider 15% of losses in energy efficiency due to the charging and discharging processes [40].

At each one-minute time slot, the available energy in the MG, $E_A^{(t)}$, is calculated as:

$$E_A^{(t)} = BE_S^{(t)} + \sum_{i=1}^{N} E_{P,i}^{(t)} \tag{1}$$

where $E_S^{(t)}$ is the energy stored in the battery at time t, B is the energy efficiency during charging and discharging processes, and $E_{P,i}^{(t)}$ represents the energy produced by the PV panel of the ith BS in the MG at time t. Similarly, the total energy demand in the MG at time t, $E_C^{(t)}$, is computed as:

$$E_C^{(t)} = \sum_{i=0}^{N} E_{C,i}^{(t)} \tag{2}$$

where $E_{C,i}^{(t)}$ denotes the energy consumed by the ith BS in the MG at time t. The BSs of a MG exchange energy through dedicated cables, to maximize the usage of the produced renewable energy. In normal operating conditions, in case the produced energy is not enough for the MG supply, i.e. $E_A^{(t)} < E_C^{(t)}$, the missing energy is drained from the power grid. If the MG produces more than what is needed for its BS supply, the exceeding energy is sold to the power grid. When a PGO occurs, the affected portion of RAN cannot draw energy from the power grid; instead, it relies solely on the available energy within the MG. In this situation, if the produced energy exceeds the energy consumption, the excess energy is stored in the battery, provided there is sufficient available capacity. During the PGO, if that amount of energy is insufficient for the BS supply, i.e. $E_A^{(t)} < E_C^{(t)}$, some or all of the BSs shut down, and the service they provide is interrupted. To make the portion of RAN as resilient as possible from PGOs, we propose several RAN resource and energy management. Their objective is the maximization of the available RAN capacity, determining which BSs are powered by the available energy. Details of the RAN resource and energy management are given in Section 4.

To evaluate the resilience of the considered portion of the RAN using our proposed methodology, we develop a simulation-based ad hoc framework. Each simulation starts at the beginning of a PGO and continues for its entire duration. The framework takes as input the date and duration of the PGO, the one-minute-granularity load on each BS in the MG, and the one-minute-granularity PV panel production during that period (see step 0 in Fig. 2). Given each BS load, the RAN energy demand is computed (step 1 in Fig. 2). Subsequently, one of the RAN resource and energy management is applied in case $E_A^{(t)} < E_C^{(t)}$, i.e. if there is not enough energy to supply all the BSs (steps 3 and 4 in Fig. 2). The simulation concludes upon the termination of the PGO (step 5 in Fig. 2).

3.1. Input data

Traffic data

Our study uses traffic data provided by a large Italian Mobile Network Operator (MNO). This dataset reports hourly load at more than 1400 BSs in Milan and the surrounding region over two months in 2015, inherently capturing the dynamics of moving users, as reflected in the measured traffic volumes and patterns across BSs. The reported BS load corresponds to aggregate traffic, resulting from the superposition of multiple service types simultaneously served at each BS. To account for the growth in mobile traffic demand in Italy from 2015 to the present, we apply a scaling factor of 27.6, as reported in [41,42]. The scaling process reflects the evolution of mobile traffic demand and usage patterns, including higher data volumes and a wider range of service types. However, modern networks show increasingly heterogeneous and volatile traffic profiles (e.g., due to high-definition video streaming and IoT connectivity). While such volatility may influence the magnitude of the resulting performance metrics, its effect is accounted for through the applied scaling process. The proposed load-based scheduling methodology, being driven by measured load levels, thus remains conceptually applicable. A detailed quantitative assessment using more recent traffic traces, with explicit per-service-type identification, is left for future work. Each BS is associated with one of these traffic traces. For each trace, we compute a "typical day" by averaging the hourly load across all days in the trace. We then process the data to achieve a one-minute granularity.

Energy outage data

Our study uses data collected via an API confidentially provided by an Italian Distribution System Operator (DSO). Given the year and energy meter ID, the API returns all outages affecting that meter during the year, including the location, duration, and start time of each outage. Our dataset includes data from Turin, Italy, covering the years 2014 to 2018. To ensure representativeness, we gathered information on users, such as energy meter locations, spread across the city. The dataset comprises over 3300 low-voltage distribution-level events, with most outages occurring between May and August and peaking in June. Outages are most frequent around 4:00 a.m. and 1:00 p.m., with durations ranging from 2 to 564 min and a median duration of under 40 min. An exponential distribution effectively approximates the fault durations. For additional details, see [23]. For this work, we use only PGOs with a duration larger than 1 min.

Energy production data

We obtained photovoltaic (PV) production data for Milan using the PVWATT tool,[1] as detailed in [43]. This tool provides data based on realistic solar irradiation patterns, reflecting the area's typical meteorological conditions over a year. The PV system considered is a fixed rooftop array with a module efficiency of 19%, system losses of 14%, a tilt angle of 30°, and an azimuth angle of 120°. The data account for power conversion losses, with a DC-to-AC ratio of 1.2 and an efficiency of 96% for the electronic components. The dataset reports hourly electricity production of PV panels in Milan, Italy, for a year, and we process it to obtain one-minute granularity.

3.2. Scenarios

In our work, we consider several MGs, whose producers and consumers are N BSs. The energy consumption of these BSs is derived from our data set, which collects the traffic load of several BSs, as mentioned above. To determine which BSs belong to each MG, we utilize a clustering approach where each sample is a 24-dimensional point representing the hourly load of a BS on a typical day. Specifically, we apply a balanced clustering method, as outlined in [44], which ensures that each cluster's size corresponds to the predetermined MG size, represented by N. We explore two scenarios for generating the MGs, as outlined below.

[1] https://pvwatts.nrel.gov/pvwatts.php

Table 3
Power requirement model parameters [36,37,45].

Parameters	Explanation	Values
P_T (W)	Radio frequency transceiver power	1.5
η	Efficiency of the power amplifier	0.5
P_B (W)	BH power link	10
P_C (W)	Cooling system power	200
P_R (W)	Rectifier power	50
P_{DSP} (W)	Digital signal processing power	1
N_A	Number of antenna sectors	1

Table 4
Summary of the proposed RAN resource management.

	Description	Comments
HLP	Maintains activity of the most loaded BSs.	Aims to maximize the served traffic.
LLP	Maintains activity of the least loaded BSs.	Aims to maximize the number of active BSs.
HLP-M	Keeps active the most loaded BSs that are already active.	Aims to maximize served traffic while minimizing BS switching events.
LLP-M	Keeps active the least loaded BSs that are already active.	Aims to maximize the number of active BSs while minimizing switching events.
SBM	Keeps active BSs capable of remaining operational for a certain period.	Avoids frequent BS switching, that arise with the battery.
LB	Ranks BSs by local energy availability. Each BS remains active if its local energy suffices; otherwise, neighboring BSs with minimal transfer losses provide support.	Minimizes energy transfer losses when they are non-negligible.

Homogeneous MG (HomMG)

This scenario represents the case of load homogeneity in geographically close areas. To create the MGs, we apply a clustering method based on the traditional k-means approach. Here, each iteration merges the two nearest clusters, based on Euclidean distance, provided it does not exceed the maximum cluster size.

Heterogeneous MG (HetMG)

This scenario reflects areas with load heterogeneity in geographical proximity, typical of locations with hotspots such as tourist attractions or parks. To do this, we apply a customized variation of k-means clustering. Unlike the traditional approach, each iteration combines the two furthest clusters, based on Euclidean distance, ensuring that the new cluster size stays within the maximum limit.

3.3. Power consumption model

As in [36], the energy consumption of a BS is computed as:

$$E_{C,i}^{(t)} = t\Big(N_a\big(P_t + P_{dsp} + \eta P_a\big) + P_r + P_c + P_{bh}\Big) \tag{3}$$

where N_a is the number of elements of the BS antenna, P_t is the power of the radio frequency transceiver, in W, P_{dsp} is power of the digital signal processing, in W, η is the efficiency of the power amplifier and P_a is the input power of the amplifier unit, in W. P_r, P_c and P_{bh} are the power drained by the rectifier, the cooling system and the backhaul link, respectively, in W. The parameter values are reported in Table 3 [36,37,45].

4. The RAN resource management

As previously mentioned, each simulation begins with the start of a PGO, which persists for its entire duration. Throughout the PGO period, the section of the RAN under consideration is unable to access energy from the power grid. It relies solely on the energy generated by the PV panels installed on each BS and stored in the battery. This means that when the produced energy is insufficient for the considered portion of the RAN, i.e., $E_A^{(t)} < E_C^{(t)}$, part or all of the BSs cannot be powered and are off rather than put into sleep mode, to avoid consuming energy required to maintain sleep state operation, interrupting the service they provide. Managing the available energy and deciding which BSs should be powered while maximizing the amount of traffic that can be handled leads to a computational problem known as the Knapsack problem, which is classified as NP-Hard. We implement various greedy approaches to determine, at each minute of the PGO, which BSs are powered and provide service, given the available energy at that time. We summarize them in Table 4.

Algorithm 1: Pseudo-code of the *HLP* and *LLP* approaches.

Input: $E_A^{(t)}$, $E_{C,b}^{(t)}$, for each BS b, order_critirion
1 $E_C^{(t)} \leftarrow 0$;
2 sort BSs using order_critirion() ;
3 **for** *each BS a* **do**
4 **if** $E_C^{(t)} + E_{C,a}^{(t)} < E_A^{(t)}$ **then**
5 turn ON BS a ;
6 $E_C^{(t)} \leftarrow E_C^{(t)} + E_{C,a}^{(t)}$;

4.1. High load priority (HLP)

The objective of this approach is to maximize the total traffic served by prioritizing the supply to the most heavily loaded BSs with the available energy (both stored and produced). Before the beginning of each minute t of the PGO, if $E_A^{(t)} < E_C^{(t)}$, the pseudo-code in Algorithm 1 is executed, assuming knowledge of the traffic load of each BS and the solar production at time t. Given the energy consumption of each BS, $E_{C,b}^{(t)}$, computed as in (3), and the available energy, $E_A^{(t)}$, we sort the BSs in descending order of load (from most to least loaded) using the function `order_criterion()` in Algorithm 1. Then, following this order, we iteratively check the BSs, keeping BS a active if the available energy in the MG is sufficient, i.e., $E_A^{(t)} \geq E_C^{(t)} + E_{C,a}^{(t)}$, where $E_C^{(t)}$ considers only the active BSs within the MG, and $E_{C,a}^{(t)}$ is the energy demand of BS a, as shown in lines 2 to 5, in Algorithm 1.

4.2. Low load priority (LLP)

This approach is similar to the previous one, but it prioritizes the activation of BSs with low traffic demand, i.e. those that consume less. At each minute t of the PGO when $E_A^{(t)} < E_C^{(t)}$, the function `order_criterion()` in Algorithm 1 sorts the BSs in descending order of load, from the least to the most loaded. Then, similarly to the previous case, iterating over the sorted BSs, we keep BS a active if the available energy is sufficient to meet the MG's energy demand, i.e., $E_A^{(t)} \geq E_C^{(t)} + E_{C,a}^{(t)}$, where $E_C^{(t)}$ considers only the active BSs within the MG and $E_{C,a}^{(t)}$ is the energy consumption of BS a (lines 2 to 5, in Algorithm 1).

4.3. High load priority with memory (HLP-M)

This approach prioritizes the supply of BSs that are active, at the previous time slot. To achieve this, at each time step t, the BSs within an MG are partitioned into two subsets: one containing the BSs that are off at time step $t-1$, $\mathcal{B}_S$, and the other, $\mathcal{B}_A$, containing the BSs that were active at time step $t-1$. We then apply the *HLP* approach to the BSs in $\mathcal{B}_A$, see Algorithm 1. We sort its BSs from the most loaded to the least loaded and we iterate over the sorted BSs, keeping active the BS a if $E_A^{(t)} \geq E_C^{(t)} + E_{P,a}^{(t)}$, where $E_C^{(t)}$ considers only the active BSs within the

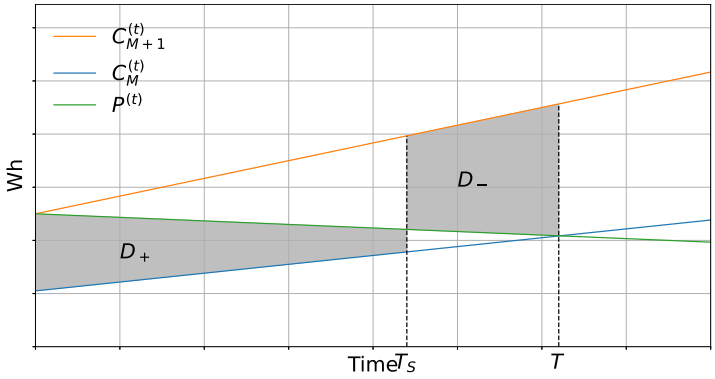

Fig. 3. Visual representation of T_S, T, when $E^{(t)}_P$ is in a decreasing phase, given $C^{(t)}_M$, $C^{(t)}_{M+1}$.

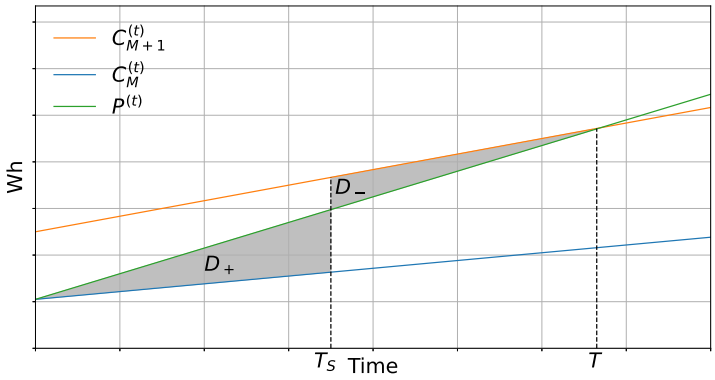

Fig. 4. Visual representation of T_S, T, when $E^{(t)}_P$ is in a increasing phase, given $C^{(t)}_M$, $C^{(t)}_{M+1}$.

MG and $E^{(t)}_{C,a}$ is the energy consumption of BS a. Then, *HLP* is executed for the BSs in $\mathcal{B}_S$. Note that at the first time slot of the PGO, the BSs are considered active from the previous time slot.

4.4. Low load priority with memory (LLP-M)

As for *HLP-M*, with this approach we prioritize the supply of BSs that are active at the previous time slot, with the objective of avoiding frequent BS switching that damages the BS hardware. At each time step t, we create the sets of off and on BSs at time $t-1$, denoted by $\mathcal{B}_S$ and $\mathcal{B}_A$, respectively. Then, we apply the *LLP* approach to the BSs in $\mathcal{B}_A$: we sort its BSs from the most loaded to the least loaded and we keep active the BS a if $E^{(t)}_A \geq E^{(t)}_C + E^{(t)}_{P,a}$, where $E^{(t)}_C$ considers only the active BSs within the MG and $E^{(t)}_{C,a}$ is the energy consumption of BS a. Finally, *LLP* is executed for the BSs in $\mathcal{B}_S$. As for *HLP-M*, at the first time slot of the PGO, the BSs are considered active from the previous time slot.

4.5. Smart battery management (SBM)

While the previous approach activates a BS as soon as the available energy $E^{(t)}_A$ is sufficient to keep it operational, this behavior can lead to frequent activation and deactivation, potentially damaging the BS hardware [46,47]. In contrast, the proposed approach activates a BS only if it can remain operational for an extended period, potentially longer than a single time slot. Practically, when the available energy is sufficient to keep M BSs active but not $M+1$, any surplus energy not consumed by the RAN is stored in the battery. Over time slots, the energy stored in the battery accumulates, eventually making it possible to activate the $(M+1)$th BS. However, if the $(M+1)$th BS is activated prematurely, it may remain active for only a single time slot due to energy unavailability, leading to frequent and undesirable BS switching.

To address this issue, we propose an energy management strategy that, while keeping M BSs active, computes T_S, the time required to accumulate sufficient energy to sustain the $(M+1)$th BS continuously from T_S to T, when the energy production alone becomes sufficient to support the additional BS. This approach ensures that the $(M+1)$th BS remains active without frequent switching.

We model the energy consumption during the PGO as a linear function of time, see green curves in Figs. 3 and 4. This is a realistic assumption if the time interval considered is sufficiently short. The energy consumption with M and $M+1$ active BSs is denoted by $C^{(t)}_M$ and $C^{(t)}_{M+1}$, respectively, and are linear with the time, as illustrated by the orange and blue curves in Figs. 3 and 4. This modeling is motivated by the observation that, over short time intervals, traffic demand growth or decline behaves linearly with time in both increasing and decreasing phases, as does energy consumption. At the beginning of each time slot t, one minute long, the algorithm tries to maintain the BS allocation of the previous time slot, $t-1$, and activate or deactivate some BSs, if the produced energy is larger or lower than what is needed, respectively. Notice that this part of the allocation considers only the produced energy at the current time slot. Practically, in this phase of the procedure, $C^{(t)}_M$ and $C^{(t)}_{M+1}$, see orange and blue curves in Figs. 3 and 4, are computed. At this point, the algorithm checks if the unused produced energy and the energy stored in the battery are enough for activating the $(M+1)$th BS. If this is the case, we check if T_S is larger than t. If this is the case, it means that we wait enough time to ensure that $(M+1)$th BS remains active up to T. If this is not the case, T_S is updated, as described below. For doing this, we distinguish two possible scenarios that differ for its computation: when energy production is in a decreasing phase (Fig. 3) and when it is in an increasing phase (Fig. 4).

4.5.1. Decreasing phase of energy production

If energy production is in a decreasing phase, the energy demand for $M+1$ BSs, defined as $C^{(t)}_{M+1} = c_{M+1} + N(t-t_0)$, exceeds the energy production, defined as $P^{(t)} = c_{M+1} + K(t-t_0)$, where $K \leq 0$. The energy demand for keeping M BSs active is modeled as $C^{(t)}_M = c_M + M(t-t_0)$. For

simplification, let $t = t - t_0$ and shift the ordinate axis by c_M, resulting in $C_M^{(t)} = Mt$, $C_{M+1}^{(t)} = c + Nt$, and $P^{(t)} = c + Kt$, where $c = c_{M+1} - c_M$ and is computed as $c = T(M - K)$. The energy stored in the battery, given by the difference between production and consumption up to time T_S, scaled by the charging efficiency E, is as follows:

$$D_+ = \int_0^{T_S} E\Big(P^{(t)} - C_M^{(t)}\Big)dt = E\Big(cT_S + \frac{K-M}{2}T_S^2\Big) \tag{4}$$

The energy needed to supply the additional $(M+1)$th BS between time T_S and T is the difference between the energy consumption of $M+1$ BSs, $C_{M+1}^{(t)}$, and production during this period:

$$D_- = \int_{T_S}^{T} \Big(C_{M+1}^{(t)} - P^{(t)}\Big)dt = \frac{N-K}{2}(T - T_S)^2 \tag{5}$$

To ensure the $(M+1)$th BS remains active from T_S to T, the energy extracted from the battery at T_S must equal the energy that is present and the battery and shortfall during this period, i.e., $EB + ED_+ = D_-$, given E the efficiency during the battery charging and discharging processes and B the energy in the battery. Using (4) and (5), we find:

$$EB + E^2\Big(cT_S + \frac{K-M}{2}T_S^2\Big) = \frac{N-K}{2}(T - T_S)^2 \tag{6}$$

Solving this second-degree equation, we select the minimum positive solution and set T_S^*, the time to wait before activating the $(M+1)$th BS, as $t + T_S$. If the equation has no solution or only negative ones, no T_S ensures that the $(M+1)$th BS can remain active until T.

4.5.2. Increasing phase of energy production

When energy production is in an increasing phase during the PGO, after time t_0, the energy consumption with M BSs, is modeled as $C_M^{(t)} = c_M + M(t - t_0)$, and the production as $P^{(t)} = c_M + K(t - t_0)$. By delaying the activation of the $(M+1)$th BS until T_S, it can remain active until time T, when energy production surpasses the RAN consumption with $M+1$ active BSs. Similarly to the previous case, we define $t = t - t_0$ and $c = c_{M+1} - c_M$, resulting in $P^{(t)} = c + Kt$, $C_M^{(t)} = Mt$, $C_{M+1}^{(t)} = c + Nt$, and $C = T(K - N)$.

The energy injected into the battery up to T_S is given by:

$$D_+ = \int_0^{T_S} E\Big(P^{(t)} - C_M^{(t)}\Big)dt = E\Big(\frac{K-M}{2}T_S^2\Big) \tag{7}$$

The energy required to supply the additional $(M+1)$th BS corresponds to the difference between the energy consumption of $M+1$ BSs and the production from T_S to T:

$$D_- = \int_{T_S}^{T} \Big(C_{M+1}^{(t)} - P^{(t)}\Big)dt = \Big(c + \frac{N-K}{2}\Big)(T^2 - T_S^2) \tag{8}$$

The time T_S is determined such that the energy extracted from the battery at T_S equals the energy shortfall from T_S to T, i.e., $EB + ED_+ = D_-$. Using (7) and (8), we have:

$$EB + E^2 T_S^2 \frac{K-M}{2} = \Big(c + \frac{N-K}{2}\Big)(T^2 - T_S^2) \tag{9}$$

As in the previous case, solving this second-degree equation yields T_S^*, and we select the minimum positive solution to determine the time to wait before activating the $(M+1)$th BS, as $t + T_S^*$. If no positive solution exists, no T_S ensures that the $(M+1)$th BS can remain active before T.

4.6. Loss based (LB)

While maximizing the managed traffic, the objective of this management is to minimize the energy loss caused by transfers between BSs along cables. To achieve this, BSs are sorted in descending order based on their local energy production. Iteratively, each BS a is kept active if its local energy is sufficient to meet its supply needs. If not, the other BSs are sorted in ascending order of the energy loss experienced between BS a and each of the others. Following this order, we check whether any of the other BSs can provide the additional energy required to activate BS a.

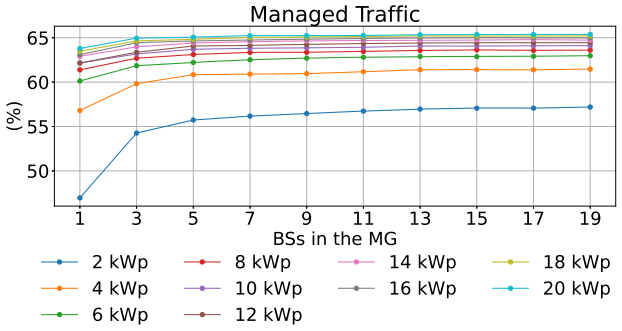

Fig. 5. *Managed traffic* with RAN resource management varying the PV panel capacity and the number of BSs within the MG.

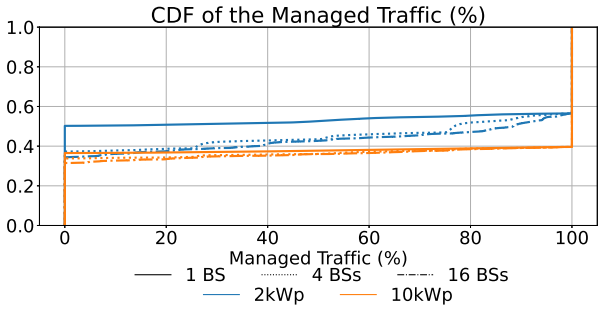

Fig. 6. CDF of the *Managed traffic*, comparing a 2 kWp (orange) and 10 kWp (blue) PV panel, with varying numbers of BSs in the MG: 1 BS (solid lines), 4 BSs (dotted lines), and 16 BSs (dashed lines). (For interpretation of the references to colour in this figure legend, the reader is referred to the web version of this article.)

Although decisions are taken on a per-time-slot basis, long-term stability over the finite power outage interval is ensured by the LLP-M, HLP-M, and SBM management mechanisms, which are designed to prevent oscillatory and unstable behavior over time.

5. Performance indicators

Managed traffic (%)

Average percentage of traffic demand that is met by the network during a PGO, since some BSs are inactive and do not provide any service because of the energy supply shortages. This metric serves as an indicator of QoS within the RAN during PGOs.

Active time to outage duration (A2D)

Average timeshare during which the BS remains operational relative to the PGO duration. In the event of a PGO, a BS is considered active and capable of providing service if there is sufficient available energy for its supply. Otherwise, the BS is off and does not provide any service.

Switch rate (SR)

Considering an MG, the total number of times any BS changes state (either from on to off or vice versa) is computed and divided by the total simulation time in minutes. It is measured in $switch/s$.

Status duration

The *Status Duration* is defined as the average time interval between two consecutive status changes (from active to off or off to active) for a BS in a given MG.

6. Numerical results

In our simulations, each PGO from our data set is applied to every MG generated as described in Section 3. The results are presented as

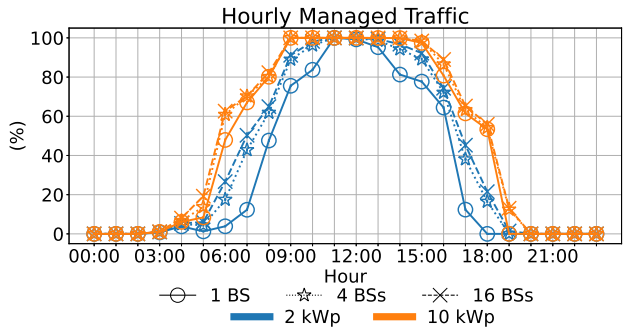

Fig. 7. Hourly managed traffic, with 2 kWp (blue) and 10 kWp (orange) PV panel capacities, considering 1 BS (circle-marked curves), 4 BSs (star-marked curves), and 16 BSs (cross-marked curves) within the MG. (For interpretation of the references to colour in this figure legend, the reader is referred to the web version of this article.)

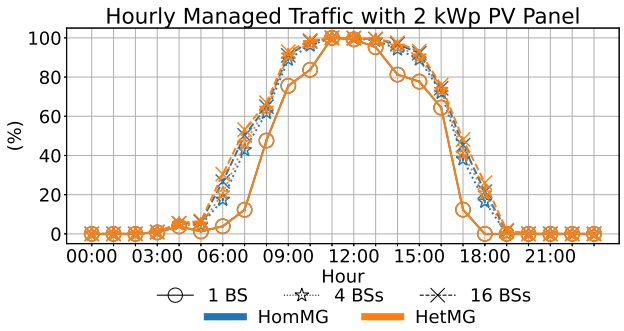

Fig. 8. Hourly managed traffic, with a 2 kWp PV panel capacity, considering 1 BS (Circle-marked curves), 4 BSs (Star-marked curves), and 16 BSs (Cross-marked curves) within the MG, in the *HomMG* (blue) and *HetMG* (orange) scenarios. (For interpretation of the references to colour in this figure legend, the reader is referred to the web version of this article.)

averages across the various simulated MGs and PGOs. Unless differently stated, we focus on the *HomMG* scenario. In the first part of the work, we assume that the losses along the power cables are negligible due to the relatively short-range distances considered in this context [48].

6.1. Efficacy of the MG

Impact of the number of BSs in the MG

This part of our work analyses the impact of the number of BSs composing the MG and the capacity of the PV panels. For doing this, we use *HLP* as RAN resource management and zero kW as the capacity of the battery in each MG. In Fig. 5, each curve in the plot is the percentage of the *Managed Traffic* with different capacities of the PV panel installed on each BS, varying, on the x-axis, the number of BSs in the MG. From the figure, we observe that the growth of the PV panel capacity increases the *Managed Traffic* during the PGO, as more energy is produced. Specifically, the *Managed Traffic* is smaller than 56%, in case the capacity of the PV panel of each BS is 2 kWp while it exceeds 64% when the capacity is 20 kWp. Additionally, the figure highlights that the rise of the number of the BSs in the MG increases the percentage of the *Managed Traffic*. This happens because when the generated energy is not enough for the MG supply, certain BSs are off and the energy produced by the PV panel of those off BSs is redistributed and utilized to power the other BSs, that can remain active. The growth of the *Managed Traffic* is significant for small PV panel systems, accounting for 17.5% with 2 kWp, but it diminishes for large ones: not exceeding 7% in the case of PV panel capacity equal to 8 kWp. Notice that a MG composed of 9 BSs, each equipped with 6 kWp, manages a larger portion of traffic compared to a single BS, equipped with a 10 or 12 kWp PV panel. Finally, the figure reveals that the *Managed Traffic* never exceeds 65%, even with large PV panel capacity and MG size, due to PGO occurrences at night when the PV panels do not produce, regardless of their capacity.

To better catch the effect of the BS number of the MG, Fig. 6 shows the CDF of the percentage of the *Managed Traffic*, in case the MG is composed of 1 BS (solid lines in the figure), 4 BSs (solid dotted in the figure) and 16 BSs (dashed lines in the figure), respectively, with PV panel capacity of 2 kWp and 10 kWp, in blue and orange. From Fig. 6, we notice that 43% and 59% of PGOs, respectively, are transparent to the provided service, with no loss of traffic when each MG is composed of a single BS. This typically occurs during daily hours. For 51% and 38% of PGOs, respectively, the percentage of *Managed Traffic* is 0%, indicating a total interruption of the service. Furthermore, for the remaining 6% and 3% of PGOs with 2 kWp and 10 kWp-equipped BSs, respectively, the *Managed Traffic* ranges between 0% and 100%. The growth of the number of BSs in the MG increases the *Managed Traffic*. Now, we focus on the PGOs that causes traffic loss when the MG is composed of a single BS, i.e. for which the *Managed Traffic* is lower than 100%, as these are the instances where QoS may be improved. Among these, the growth in the MG size increases the *Managed Traffic* in 32% and 38% of PGOs, for MG composed of 4 and 16 BSs, respectively, with 2 kWp-equipped BSs, compared to the case with solated BSs (MG composed of a single BS). For 22% and 23% of these instances, the network can manage at least 50% of the traffic demand. Results, if the BSs are equipped with a 10 kWp PV panel, are similar but with slightly less sensitivity to the MG size variation. Focusing on PGOs with *Managed Traffic* lower than 100% with single BS MGs, the *Managed Traffic* improves in 10% and 20% of cases, when the MG size is 4 and 16 BSs, respectively. Additionally, among these PGOs, it is larger than 50% in 9% of cases.

Now, we analyze the impact of the MG size, during the different hours of the day. In Fig. 7, the *Managed Traffic* is plotted, when the PV panel of each BS is 2 kWp and 10 kWp, in blue and orange, respectively, varying the number of BSs in the MG, denoted by different markers. Each point of the curves in the figure is the *Managed Traffic*, computed considering only the PGOs that start at the corresponding hour, which varies on the x-axis. From the figure, we identify three distinct areas. First, until 3:00 a.m. and after 20:00, the energy which is produced by the PV panel is never sufficient, because of lack of energy production. Consequently, the PV panel capacity or the number of BSs in the MG have no impact on the network resilience during these periods. Second, at 11:00 and 12:00, the portion of RAN can manage almost all the traffic demand, as the PV panel always produces enough energy during these hours, regardless of the PV panel capacity and/or how many BSs compose the MG. Finally, from 4:00 to 10:00 and between 13:00 and 20:00, the network performance is strictly related to the PV panel capacity and/or the number of BSs in the MG. In these periods, increasing the MG size from 1 to 4 BSs raises the *Managed Traffic* by an amount that is between 12% and 352%, improving from values in the range of 1-83% to 4-96%. Further increasing the MG size to 16 BSs results in *Managed Traffic* gains ranging from 6% to 590%, with the largest improvement observed at 6:00, where *Managed Traffic* increases from 4% (for 1 BS) to 27% (for 16 BSs). Similar trends are observed when each BS is equipped with a 10 kWp PV panel: MGs composed of 4 and 16 BSs improve *Managed Traffic* by up to 64% (from 8% to 14%) and 129% (from 8% to 19%), respectively, compared to isolated BSs.

Impact of the traffic patterns

In this part of the work, we analyze the performance during the PGOs in scenarios that differ for the heterogeneity of the traffic demand within the MG. In Fig. 8, the hourly *Managed traffic* is presented, when *HLP* is the used RAN resource management and zero kW the capacity of the battery in each MG. The blue curves are the results for the *HomMG* scenario, i.e. where the BSs in the MG exhibit a similar traffic demand profile, typical of a scenario that operates under the assumption of load homogeneity in close geographical areas. The orange curves in the

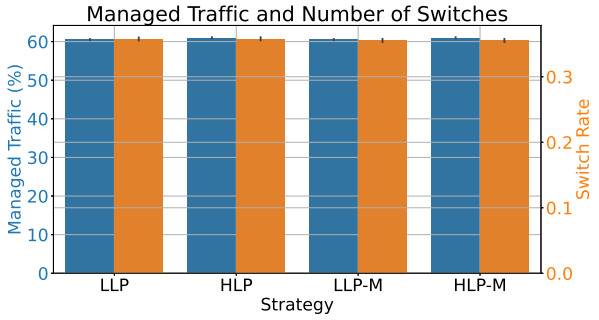

Fig. 9. *Managed traffic* (blue, left y-axis) and *Switch Rate* (orange, right y-axis) with a 4 kWp PV panel and 8 BSs within the MG, under different RAN resource management strategies. (For interpretation of the references to colour in this figure legend, the reader is referred to the web version of this article.)

figure are for the *HetMG* scenario, characterized by MGs with BSs having dissimilar traffic demand shapes. As mentioned in Section 3, this scenario reflects areas with heterogeneous loads within close geographical proximity, typical of areas with hotspots such as tourist attractions or parks. The curves denoted by the circles, stars, and crosses are the results in case the number of BSs in the MG is equal to 1, 4, and 16, respectively. When the MG is composed of a single BS, i.e. there is no energy exchange neither RAN resource management, the results obtained in the *HomMG* and *HetMG* scenarios are identical, as expected. For MG composed of 4 and 16 BSs, the situation is different. Until 5:00, after 19:00, and between 11:00 and 12:00, the *Managed Traffic* is identical, regardless of the scenario or number of BSs in the MG. This is due to the lack of energy generation during these time intervals or the large energy generation between 11:00 and 12:00, which is always sufficient for BS supply, as explained above (see Fig. 7). Between 6:00 and 10:00 and from 13:00 to 18:00, the figure shows that the heterogeneity of the traffic demand profiles of the BSs in the MG impacts the *Managed Traffic*. It is slightly larger (between 0.05% and 26%) in the *HetMG* scenario than in the *HomMG* one. This is because in the *HetMG* scenario, BSs have peaks and low traffic periods misaligned, making more likely energy exchange among the BSs.

6.2. Impact of the different RAN management approach

We now discuss the impact of different RAN resource and energy management approaches, as detailed in Section 3. For this analysis, we consider MGs consisting of 8 BSs, each equipped with a 4kW PV panel system and no battery storage (0kWh). Fig. 9 depicts the *Managed Traffic*, on the lft y-axis, and the *Switch Rate*, on the right y-axis, across the various RAN management approaches. From the figure, we observe that the impact of each approach is nearly identical for both KPIs. Specifically, the *Managed Traffic* is 61% and 60.5% when prioritizing the most and least loaded BSs, respectively, and the *Switch Rate* is 0.36 for both. This similarity arises because the traffic demands at the BSs are comparable, rendering the prioritization approach irrelevant. Similarly, employing the *memory* variation results in no significant performance differences. This is due to the minimal variation in traffic demand over time at each BS. Consequently, if a BS exhibits the lowest (or highest) traffic demand at the start of the PGO and is kept active for this reason, it typically maintains the lowest (or highest) traffic demand throughout the PGO.

6.3. Usage of batteries

We now consider a scenario in which each MG includes a set of lead-acid battery units (see Section 3), resulting in a total storage capacity of 93 kWh. Fig. 10 presents the percentage of *Managed Traffic*, the *Switch Rate*, and the *Status Duration* for a single MG composed of 8 BSs. The strategies compared are *HLP* with no battery (shown as *No Battery* in the figures), *HLP* with a battery, and *SBM*, represented in orange, blue, and green, respectively. The results indicate a slight increase in *Managed Traffic* when moving from the *No Battery* case to *HLP with Battery* or *SBM*, rising from 61% to 62%. However, *SBM* slightly reduces *Managed Traffic* to 61.5%, due to its stricter conditions for activating a BS compared to *HLP*.

Table 5
Managed traffic with *HLP*, *L-B*, and optimal energy and RAN resource allocation, considering different MG physical topologies, using a 4 kWp PV panel and 8 BSs within the MG.

Strategy	Managed Traffic Volume (%)
HLP Bus	59.81
HLP Star	60.55
L-B Bus	59.93
L-B Star	60.19
Opt Bus	60.41
Opt Star	60.57

Additionally, Fig. 10 highlights distinct differences in switching behavior across the strategies. The *No Battery* baseline exhibits minimal *Switch Rate*. Although BSs are deactivated whenever locally generated energy falls below the consumption level, in the configurations with batteries (*HLP with Battery* and *SBM*), the stored energy can later enable the temporary reactivation of one or more previously switched-off BSs once sufficient energy has accumulated. This charge-discharge cycle introduces additional switching events, leading to a higher overall *Switch Rate* compared to the *No Battery* case. Both *HLP with Battery* and *SBM* therefore show an increase in switching events, with the latter demonstrating a more controlled and efficient switching pattern, likely due to its more advanced management approach. This behavior motivates the longer *Status Duration* observed with *SBM* when compared to *HLP with Battery*, highlighting the effectiveness of our proposal in preventing frequent BS switching.

The results indicate that using batteries for energy storage during PGOs slightly improves the service quality. Nonetheless, this approach leads to an increase in BS switching, which can be mitigated through effective management strategies that focus on optimizing the battery's operational dynamics.

6.4. Impact of the geographical position of the PV panel installation

In this part of the work, we assume that the BSs within the MG are far enough apart to assume negligible losses along the power cables unrealistic. We analyze two possible topologies: bus and star. For the bus topology, BSs are arranged in descending order of total load, numbering BSs from 1 to 8, with BS 1 being the most loaded and BS 8 the least. Energy efficiency along the cables in the star topology is assumed to be 80% per cable line between each pair of BSs. In contrast, for the bus topology, efficiency is modeled as $0.8^{|i-j|}$ for the cable connecting BS i to BS j. We adopt this exponential decay model as a simplified abstraction to capture the idea that an increase in physical distance corresponds to a greater power loss [49,50]. While a physics-based model incorporating cable resistance, current flow, and line length would provide more precise loss estimates, this model preserves the qualitative comparison between bus and star topologies, that longer transmission paths in the bus topology lead to higher cumulative losses.

Fig. 11 illustrates the *Managed Traffic* as the number of BSs in the MG varies. The results are shown for three scenarios: when each BS is equipped with a 4 kWp PV panel and the MG topology is a star (orange) or bus (green), and when the BSs are close enough to have negligible cable losses (blue). As expected, increasing the distance between BSs reduces the *Managed Traffic* due to energy losses during power transfer,

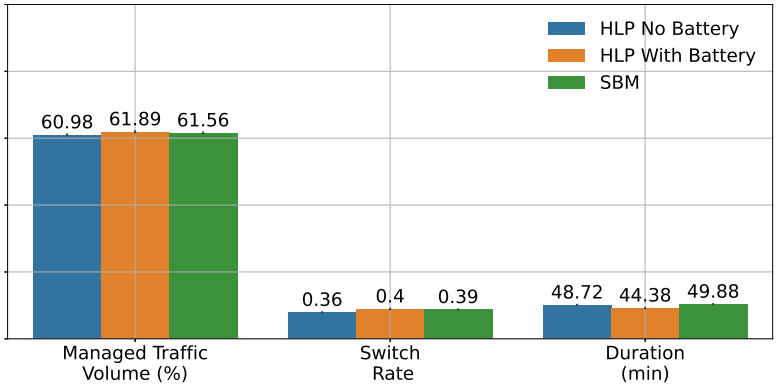

Fig. 10. *Managed traffic*, *switch rate* and *average duration* with a 4 kWp PV panel and 8 BSs within the MG, under different RAN resource management strategies.

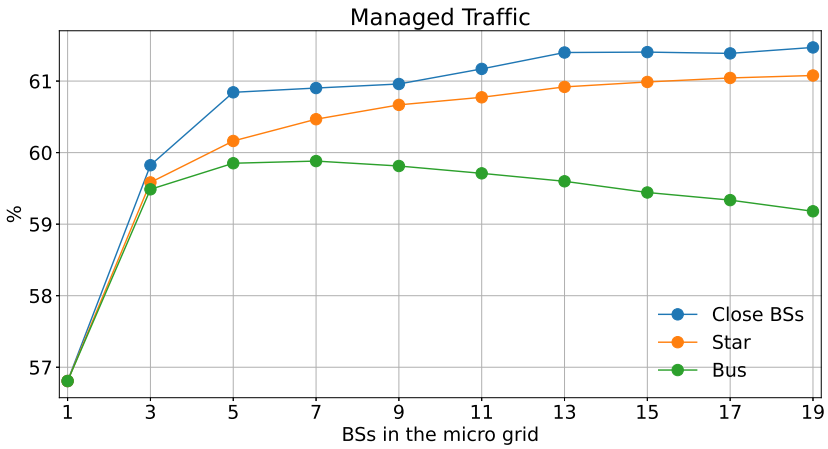

Fig. 11. *Managed traffic* with a 4 kWp PV panel capacity, varying the number of BSs in the MG and using different MG topologies.

with this reduction reaching up to 3.5%. Additionally, while the *Managed Traffic* for the star topology (orange curve in Fig. 11) grows almost linearly as the MG size increases from 1 to 7 BSs and then stabilizes (as seen in Fig. 5), the behavior for the bus topology is different. Specifically, starting from 9 BSs per MG, the *Managed Traffic* begins to decrease. This occurs because, in the bus topology, increasing the number of BSs increases the potential maximum distance between them, leading to greater energy losses along the cables and thus reducing the usable energy.

Next, we analyze a single MG from our dataset, composed of 8 BSs, each equipped with a 4 kWp PV panel. Table 5 presents the *Managed Traffic* for the *HLP* and *L-B* resource allocation strategies, as well as the optimal solution, considering both bus and star topologies. The results demonstrate that the *Managed Traffic* is nearly identical across all strategies, highlighting that our proposed approaches perform almost as well as the optimal solution. Furthermore, the star topology consistently achieves slightly better QoS compared to the bus topology.

In this part of the work, we investigate the impact of PV panel placement in scenarios where some BSs cannot host them, for instance, due to installation space constraints. Fig. 12a illustrates the *Managed Traffic* obtained in a setup with 8 BSs within the MG, where a single 32 kWp PV panel is installed on the BS indicated on the x-axis. As mentioned above, in the bus topology, BSs are arranged in descending order of total load. The figure shows the *Managed Traffic* for the *HLP*, *L-B*, and optimal resource and energy allocation strategies. These are represented by blue and orange curves, green and red curves, and purple and brown curves for star and bus topologies, respectively. The results confirm that the *Managed Traffic* is consistently higher in the star topology compared to the bus topology for all strategies. Among the strategies, the *L-B* approach achieves nearly identical *Managed Traffic* to the optimal solution, with values ranging between 56% and 60%. These values are comparable to scenarios where each BS has its own PV panel (refer to Table 5). Furthermore, while relocating the PV panel between BSs has negligible impact on performance in the star topology, the bus topology shows slight variations, with *Managed Traffic* oscillating between 56% and 60%. Specifically, placing the PV panel at BSs located in the middle of the MG yields better performance than placing it at the edges, as the maximum energy transfer distance is shorter in the former case. When the *HLP* strategy is used, the *Managed Traffic* significantly decreases compared to *L-B*, with values never exceeding 40%. This reduction is due to the *HLP* strategy prioritizing the activation of the most loaded BSs, regardless of energy losses during transfer.

As can be noticed in Fig. 12b, similar observations can be done for the scenario where there are 2 PV panels, one on the most loaded BS (BS 1) and the other on one of the remaining BSs, indicated on the x-axis in Fig. 12b. Notice that, while the optimal solution and the L-B approach provide almost the same *Managed Traffic* as when there is a single PV panel, in the case of *HLP* usage, it improves by up to 43%, since each BS reduces its distance from the PV panel.

These findings highlight the critical role of topology, PV panel placement, and resource allocation strategies in mitigating energy losses and enhancing system resilience, particularly under constrained PV panel placement scenarios.

6.5. Comparison with the energy battery as back-up system

In this part of our study, we compare the performances obtained with the MG, using *HLP* and no energy battery, to the traditional solution, which involves using an energy battery as a power backup system, with a capacity of 1.2 kWh. We consider a maximum Depth of Discharge

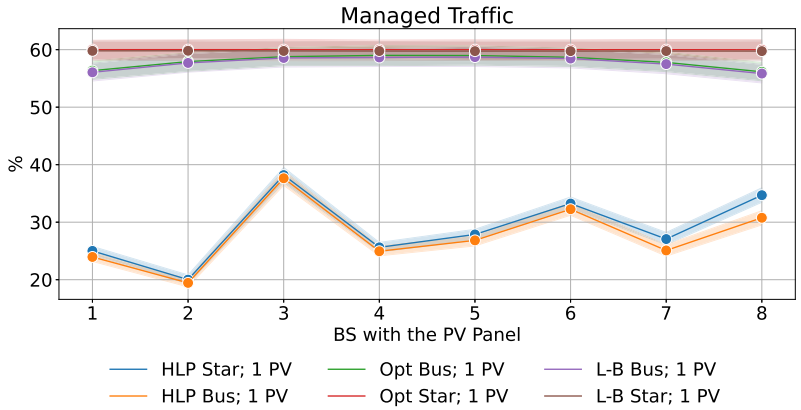

(a) 1 PV panel

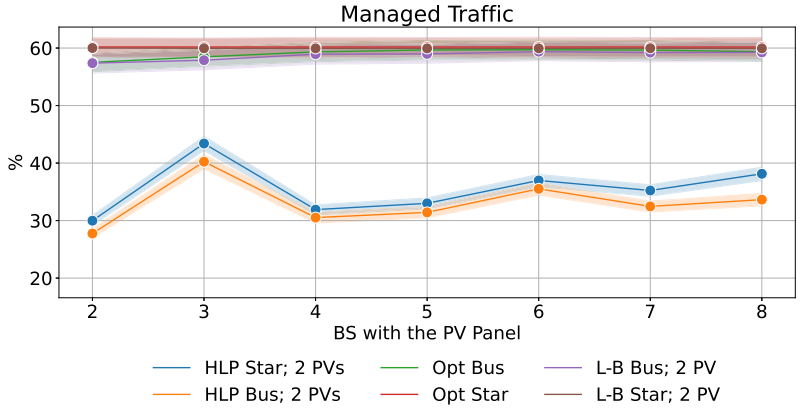

(b) 2 PV panels

Fig. 12. *Managed traffic* with a 4 kWp PV panel capacity and 8 BSs within the MG, analyzing the impact of moving the PV panel installation location (x-axis), considering scenarios where the PV panel is installed on a single BS (a) or shared between BS 1 and another BS (b), for different topologies and energy and RAN resource allocation approaches.

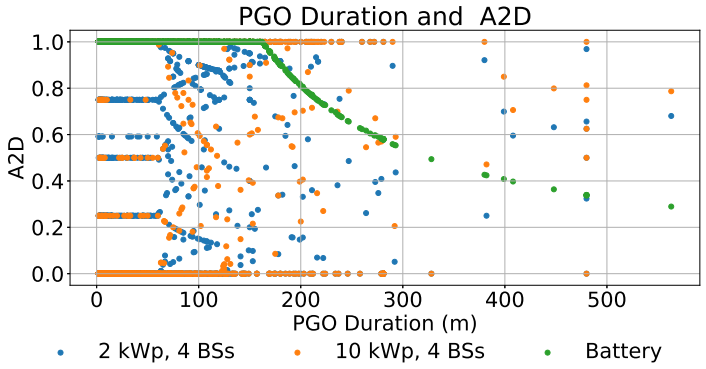

Fig. 13. *A2D* varying the PGO duration, in minutes.

(DOD) of 70% for this battery. This DOD value allows the battery to operate for more than 500–600 cycles before needing replacement [38,39]. Additionally, we account for losses of 15% in energy efficiency due to the charging and discharging processes [40]. Fig. 13 combines the PGO duration, in minutes, and the *A2D*, that is the fraction of time the BSs remains active relative to the PGO duration. Each PGO is represented with a marker positioned so that the x-axis value corresponds to the PGO duration and the y-axis value corresponds to the *A2D* when that PGO occurs. In the figure, the blue and orange points are for the MG composed of 4 BSs, each equipped with a PV panel system whose capacity is 2 kWp and 10 kWp, respectively; the green points are for the energy battery backup system solution. From Fig. 13, we notice that the PGO duration has no impact on the *A2D* in the MG. Indeed, as discussed in the previous sections, the performance is strictly dependent on the hour of the day, see Fig. 7. When an energy battery is employed as a backup system, the *A2D* is larger than when there is the MG. In this case, each BS remains active for almost the entire duration of the PGO. Nevertheless, as soon as the battery is depleted, each BS turns off. This implies that the resulting performance is strictly dependent on the duration of the PGO. For PGOs longer than 160 min, the energy battery keeps a BS

active for a shorter time than the MG cases, if the PGO occurs during daily hours.

7. Lesson learnt

In this section, we discuss the key findings that have emerged from our work.

Our study addresses the lack of energy provisioning from the power grid in the RAN by treating BSs as both producers and consumers within a MG. These BSs are equipped with PV panels and energy storage batteries, exchanging energy through dedicated power cables. We propose different RAN resource management strategies to determine which BSs should be activated during PGOs, particularly when the energy produced within the MG is insufficient to meet RAN demands. These strategies make decisions based on traffic load, available energy production, and power losses along the cables.

First, our results highlight that the MG is particularly effective during PGOs occurring outside peak hours and periods of zero PV panel production. During these times, energy exchange enables a subset of BSs within the MG to remain operational, whereas, without the MG, they would otherwise be turned off due to insufficient energy availability. Additionally, adopting the MG paradigm allows for the installation of smaller PV panels without compromising service quality. For example, the performance achieved with PV panels smaller than 6 kWp, when combined with the MG, is comparable to that obtained with 12 kWp PV panels, making this approach more feasible in terms of installation space requirements.

Second, our evaluation demonstrates that service quality is minimally affected by variations in traffic demand profiles, leading to nearly identical performance across all energy and resource allocation strategies based on traffic patterns. Similarly, utilizing batteries for energy storage during PGOs has a limited impact on service quality but increases BS switching. This effect can be mitigated through effective management strategies aimed at optimizing the battery's operational dynamics.

Finally, in scenarios with a non-uniform distribution of energy production capacity, managing energy while considering cable losses is crucial to preventing energy waste, which would otherwise degrade service quality. In such cases, the placement of energy production units should minimize the distance to all BSs to enhance efficiency.

8. Conclusion

In this work, to address the lack of energy provisioning from the power grid in the RAN, we adopt the MG paradigm, envisioning a set of PV panel-equipped BSs as both energy consumers and producers within a MG. These BSs can exchange energy through dedicated power cables.

Our evaluation considers various factors, including the number of BSs in each MG, PV panel capacity, the timing of PGOs, BS traffic demand profiles, PV panel placement, and distances between BSs, while testing our proposed energy and RAN management approaches. The results reveal that, although outcomes heavily depend on the time of day, our methodology, which manages BSs and available energy as MGs, enhances QoS, increasing the hourly Managed Traffic by more than 300% compared to the case where each BS operates independently, without MG coordination.

Furthermore, we demonstrate that the performance of our methodology is largely unaffected by the traffic demand profiles of BSs within the MG or the duration of PGOs. Finally, the results highlight that, when PV panel capacity cannot be evenly distributed among BSs, effective energy management, taking cable losses into account and strategically placing PV panels centrally within the MG, is crucial for optimizing performance.

Future research will investigate the technical and economic feasibility of implementing dedicated cables for energy exchange within the microgrid, including an assessment of infrastructure costs, deployment scenarios, and potential integration with existing networks, clarifying whether the proposed solution is better suited for new, dense deployments or for retrofitting existing infrastructures, and exploring opportunities to leverage existing power lines or shared infrastructure to enhance practicality and scalability. In addition, we aim to extend the proposed framework by incorporating differentiated scheduling mechanisms that dynamically prioritize various traffic classes (e.g., video streaming, IoT, or background data) according to their latency and throughput requirements.

CRediT authorship contribution statement

Greta Vallero: Writing – review & editing; **Michela Meo:** Project administration; **Umberto Brozzo Doda:** Methodology.

Data availability

The data that has been used is confidential.

Declaration of interests

The authors declare that they have no known competing financial interests or personal relationships that could have appeared to influence the work reported in this paper.

Acknowledgment

This paper was supported by the European Union under the Italian National Recovery and Resilience Plan (NRRP) of NextGenerationEU, partnership on "Telecommunications of the Future" (PE00000001 - program "RESTART", Focused Project R4R).

References

[1] E.U. A.f. Network, S. Information, ENISA - Annual Report Telecom Security Incidents 2021, Technical Report July, 2021. https://doi.org/10.2824/528645
[2] H. Jones, Going beyond reliability to robustness and resilience in space life support systems, 50th International Conference on Environmental Systems, 2021.
[3] V. Suryaprakash, I. Malanchini, Reliability in future radio access networks: from linguistic to quantitative definitions, in: 2016 IEEE/ACM 24th International Symposium on Quality of Service (IWQoS), IEEE, 2016, pp. 1–2.
[4] J.P.G. Sterbenz, D. Hutchison, E.K. Çetinkaya, A. Jabbar, J.P. Rohrer, M. Schöller, P. Smith, Resilience and survivability in communication networks: strategies, principles, and survey of disciplines, Comput. Netw. 54 (8) (2010) 1245–1265.
[5] P.E. Heegaard, K.S. Trivedi, Network survivability modeling, Comput. Netw. 53 (8) (2009) 1215–1234.
[6] S. Kaada, M.L.A. Morel, G. Rubino, S. Jelassi, Resilience analysis and quantification method for 5G-radio access networks, in: 2022 13th International Conference on Network of the Future (NoF), IEEE, 2022, pp. 1–9.
[7] A. Masaracchia, V. Sharma, M. Fahim, O.A. Dobre, T.Q. Duong, Digital twin for open ran: towards intelligent and resilient 6G radio access networks, IEEE Commun. Mag. 61 (11) (2023) 112–118.
[8] A. Bhattacharyya, S. Ramanathan, A. Fumagalli, K. Kondepu, Towards disaggregated resilient 5G radio access network: a proof of concept, in: 2023 IEEE 9th International Conference on Network Softwarization (NetSoft), IEEE, 2023, pp. 396–401.
[9] L. Weedage, S.R.C. Magalhães, C. Stegehuis, S. Bayhan, On the resilience of cellular networks: how can national roaming help?, IEEE Trans. Netw. Serv. Manage. 21 (2) (2024) 1702–1714.
[10] J.S. Panchal, R.D. Yates, M.M. Buddhikot, Mobile network resource sharing options: performance comparisons, IEEE Trans. Wireless Commun. 12 (9) (2013) 4470–4482.
[11] U.S. Government, Federal register / Vol. 89, No. 70 / Thursday, April 11, 2024 / rules and regulations, 2024. Accessed: 2024-11-14, https://www.govinfo.gov/content/pkg/FR-2024-04-11/pdf/2024-07402.pdf.
[12] S.S. o.S. Communications, I.P.o. Ukraine, National roaming launch in Ukraine, 2024. Accessed: 2024-11-14, https://cip.gov.ua/en/news/v-ukrayini-zapuskayut-nacionalnii-rouming.
[13] A. Cabrera-Tobar, F. Grimaccia, S. Leva, Energy resilience in telecommunication networks: a comprehensive review of strategies and challenges, Energies 16 (18) (2023) 6633.
[14] IEA, Unlocking the potential of distributed energy resources, 2022. License: CC BY 4.0, https://www.iea.org/reports/unlocking-the-potential-of-distributed-energy-resources.
[15] IEA, World energy outlook 2022, 2022. License: CC BY 4.0 (report); CC BY NC SA 4.0 (Annex A), https://www.iea.org/reports/world-energy-outlook-2022.
[16] IEA, Global energy and climate model, 2023, (https://www.iea.org/reports/global-energy-and-climate-model). License: CC BY 4.0.

[17] C. Marnay, S. Chatzivasileiadis, C. Abbey, R. Iravani, G. Joos, P. Lombardi, P. Mancarella, J. Von Appen, Microgrid evolution roadmap, in: 2015 International Symposium on Smart Electric Distribution Systems and Technologies (EDST), IEEE, 2015, pp. 139–144.
[18] J. Shi, L. Ma, C. Li, N. Liu, J. Zhang, A comprehensive review of standards for distributed energy resource grid-integration and microgrid, Renew. Sustain. Energy Rev. 170 (2022) 112957.
[19] N. Piovesan, D. López-Pérez, M. Miozzo, P. Dini, Joint load control and energy sharing for renewable powered small base stations: a machine learning approach, IEEE Trans. Green Commun. Netw. 5 (1) (2020) 512–525.
[20] G. Vallero, D. Renga, M. Meo, M.A. Marsan, Greener RAN operation through machine learning, IEEE Trans. Netw. Serv. Manage. 16 (3) (2019) 896–908.
[21] G. Perin, M. Berno, T. Erseghe, M. Rossi, Towards sustainable edge computing through renewable energy resources and online, distributed and predictive scheduling, IEEE Trans. Netw. Serv. Manage. 19 (1) (2021) 306–321.
[22] P.W.D. Bishop, S.J. Barrett, I.D. Harris, Managing projected power outage at mobile radio base sites, 2013. US Patent 8,489,154.
[23] G. Vallero, E. Pristeri, M. Meo, Coping with power outages in mobile networks, in: 2020 Mediterranean Communication and Computer Networking Conference (MedComNet), IEEE, 2020, pp. 1–4.
[24] G. Vallero, M. Meo, Microgrid for radio access network resilience, in: 2024 22nd Mediterranean Communication and Computer Networking Conference (MedComNet), 2024, pp. 1–8. https://doi.org/10.1109/MedComNet62012.2024.10578214
[25] A. Mauthe, D. Hutchison, E.K. Cetinkaya, I. Ganchev, J. Rak, J.P.G. Sterbenz, M. Gunkelk, P. Smith, T. Gomes, Disaster-resilient communication networks: principles and best practices, in: 2016 8th International Workshop on Resilient Networks Design and Modeling (RNDM), IEEE, 2016, pp. 1–10.
[26] Y. Xu, Y. Xing, Q. Huang, J. Li, G. Zhang, O. Bamisile, Q. Huang, A review of resilience enhancement strategies in renewable power system under HILP events, Energy Rep. 9 (2023) 200–209.
[27] H. Farooq, M.S. Parwez, A. Imran, Continuous time Markov chain based reliability analysis for future cellular networks, in: 2015 IEEE Global Communications Conference (GLOBECOM), IEEE, 2015, pp. 1–6.
[28] A. Cabrera-Tobar, F. Grimaccia, S. Leva, Energy resilience in telecommunication networks: a comprehensive review of strategies and challenges, Energies 16 (18) (2023) 6633. https://doi.org/10.3390/EN16186633
[29] TIM Emilia Romagna - Alluvione. https://www.gruppotim.it/it/gruppo/chi-siamo/news/TIM-EMILIAROMAGNA-ALLUVIONE.html.
[30] H. Saboori, Enhancing resilience and sustainability of distribution networks by emergency operation of a truck-mounted mobile battery energy storage fleet, Sustain. Energy Grids Netw. 34 (2023) 101037.
[31] M. Deruyck, W. Joseph, E. Tanghe, L. Martens, Reducing the power consumption in LTE-advanced wireless access networks by a capacity based deployment tool, Radio Sci. 49 (9) (2014) 777–787.
[32] L.M.P. Larsen, H.L. Christiansen, S. Ruepp, M.S. Berger, Toward greener 5G and beyond radio access networks-a survey, IEEE Open J. Commun. Soc. 4 (2023) 768–797.
[33] J. Lorincz, Z. Klarin, D. Begusic, Advances in improving energy efficiency of fiber–wireless access networks: a comprehensive overview, Sensors 23 (4) (2023) 2239.
[34] M.R. Aktar, M.D.S. Anower, M.Z.I. Sarkar, A.S.M. Sayem, M.R. Islam, A.I. Akash, M.R.A. Rume, G. Moloudian, A. Lalbakhsh, Energy-efficient hybrid powered cloud radio access network (C-RAN) for 5G, IEEE Access 11 (2023) 3208–3220.
[35] J. Franceschi, J. Rothkop, G. Miller, Off-grid solar PV power for humanitarian action: from emergency communications to refugee camp micro-grids, Procedia Eng. 78 (2014) 229–235.
[36] G. Castellanos, S. De Gheselle, L. Martens, N. Kuster, W. Joseph, M. Deruyck, S. Kuehn, Multi-objective optimisation of human exposure for various 5G network topologies in Switzerland, Comput. Netw. 216 (2022) 109255.
[37] M. Matalatala, M. Deruyck, E. Tanghe, L. Martens, W. Joseph, Simulations of beamforming performance and energy efficiency for 5G mm-wave cellular networks, in: 2018 IEEE Wireless Communications and Networking Conference (WCNC), IEEE, 2018, pp. 1–6.
[38] C. Mi, M.A. Masrur, Hybrid Electric Vehicles: Principles and Applications with Practical Perspectives, John Wiley & Sons, 2017.
[39] M. Jafari, G. Platt, Z. Malekjamshidi, J.G. Zhu, Technical issues of sizing lead-acid batteries for application in residential renewable energy systems, in: 2015 4th International Conference on Electric Power and Energy Conversion Systems (EPECS), IEEE, 2015, pp. 1–6.
[40] H. Gharavi, R. Ghafurian, IEEE recommended practice for sizing lead-acid batteries for stand-alone photovoltaic (PV) systems IEEE std 1013–2007, in: Proc. IEEE, 99, 2011, pp. 917–921.
[41] A. A. p. l. G.N. Comunicazioni, Osservatorio Sulle Comunicazioni N.4/ 2018, Technical Report N.4/2018, AGCOM - Autorita per le Garanzie Nelle Comunicazioni, 2018.
[42] A. A. p. l. G.N. Comunicazioni, Osservatorio Sulle Comunicazioni N.4/ 2023, Technical Report N.4/2023, AGCOM - Autorita per le Garanzie Nelle Comunicazioni, 2023.
[43] A.P. Dobos, PVWatts Version 5 Manual, Technical Report, National Renewable Energy Lab.(NREL), Golden, CO (United States), 2014.
[44] M.I. Malinen, P. Fränti, Balanced k-means for clustering, in: Structural, Syntactic, and Statistical Pattern Recognition: Joint IAPR International Workshop, S+SSPR 2014, Joensuu, Finland, August 20–22, 2014. Proceedings, Springer, 2014, pp. 32–41.
[45] M. Matalatala, M. Deruyck, S. Shikhantsov, E. Tanghe, D. Plets, S. Goudos, K.E. Psannis, L. Martens, W. Joseph, Multi-objective optimization of massive MIMO 5G wireless networks towards power consumption, uplink and downlink exposure, Appl. Sci. 9 (22) (2019) 4974.
[46] G. Vallero, M. Deruyck, M. Meo, W. Joseph, Base station switching and edge caching optimisation in high energy-efficiency wireless access network, Comput. Netw. 192 (2021) 108100.
[47] L. Chiaraviglio, F. Cuomo, M. Listanti, E. Manzia, M. Santucci, Fatigue-aware management of cellular networks infrastructure with sleep modes, IEEE Trans. Mob. Comput. 16 (11) (2017) 3028–3041.
[48] M.H. Nguyen, T.K. Saha, Power loss evaluations for long distance transmission lines, in: Australian Geothermal Energy Conference, 2009, pp. 307–312.
[49] K.E. GmbH, AWG table - American strand construction, 2025. Accessed: 2025-11-19, https://www.kbe-elektrotechnik.com/en/service/awg-table/.
[50] R. Khan, N.N. Schulz, M. Nasir, Distribution loss analysis of dc microgrids for rural electrification, in: 2019 IEEE Global Humanitarian Technology Conference (GHTC), IEEE, 2019, pp. 1–8.